Contributions to the magnetospheric parallel electric field

C.R. Stark, A.P. Cran-McGreehin and A.N. Wright

Stark, C.R., et al. 2011. Contributions to the magnetospheric parallel electric field. *Journal of Geophysical Research: Space Physics.* 116(A7). doi: 10.1029/2010JA016270

Contributions to the magnetospheric parallel electric field

C. R. Stark, A. P. Cran-McGreehin and A. N. Wright

School of Mathematics and Statistics, University of St Andrews, St Andrews, Scotland, UK.

C. R. Stark, Solar and Magnetospheric Group, School of Mathematics and Statistics, University of St Andrews, St Andrews, KY16 9SS, Scotland, UK. (craig@mcs.st-and.ac.uk)

Abstract. Upward field-aligned currents and their associated parallel electric fields couple the ionosphere to the magnetosphere. It is desirable to know how such a potential drop is distributed along the flux tube, what controls its variation and how it is balanced by the plasma. By considering the motion of the ionospheric and magnetospheric electrons and ions, under the influence of electrostatic and magnetic mirror forces, a quasi-steady state, quasi-neutral electric field distribution along the magnetic flux tube can be obtained. A feature of the potential profiles is the occurrence of a potential jump, that splits the profile into three distinct regions: below the jump; within the jump and above the jump. Within a kinetic framework, we analyse how the plasma velocity distributions evolve along the flux tube, taking into account ionospheric, magnetospheric, mirroring and precipitating electron populations. By calculating the moments of the governing Vlasov equation we ascertain what balances the parallel electric field ($E_\parallel$) and how it is maintained, establishing a dynamical equilibrium. Our calculations show that (1) Earthward of the jump $E_\parallel \approx -(p_\perp/enB)\nabla_\parallel B$ associated with the ionospheric electrons, except for at the base of the F region where $p_\parallel$ contributions become more significant; (2) Within the jump magnetosphere electrons dominate and $E_\parallel \approx -(1/en)\nabla_\parallel p_\parallel$; (3) Above the jump mirroring magnetospheric electrons make a principal contribution of $E_\parallel \approx -(1/en)\nabla_\parallel p_\parallel$, with a secondary contribution of $-(p_\perp - p_\parallel)\nabla_\parallel B/(ne)$ becoming comparable beyond $\approx$ 3 R_E. Additionally, we found that although the precipitating electrons carry the field-aligned current it is the mirroring popula-

tion that determines where $E_{\parallel}$ is concentrated, and hence where precipitating electrons are accelerated.

1. Introduction

Parallel electric fields and their associated field-aligned currents are key in coupling the hot, tenuous magnetosphere to the cool, dense ionosphere. They are responsible for the observed aurora and play a significant role in the global circuitry network surrounding the earth. It remains one of the outstanding problems in magnetospheric physics to fully understand the origin and structure of parallel electric fields. Observations have suggested that elongated, U-shaped potential structures straddling the magnetic field are responsible for the parallel fields. It is believed that the required parallel potential drop ($\sim$ 1 kV) is distributed over a large length scale ($\sim 10^3$ km) however, observations of large-amplitude electric fields ($\sim$ 25 to 300 mV/m) suggest that in some instances a significant fraction of the total potential drop occurs over a much smaller length scale ($\sim$ 10 km) close to the earth ($\sim$ 1000 km) [*Mozer and Hull*, 2001; *Hull et al.*, 2003a, b; *Chaston et al.*, 2007; *Ergun et al.*, 2000, 2001, 2002].

A significant challenge is understanding how the electric field varies as a function of position along the magnetic field and what controls that variation. Initial modelling of magnetospheric fields by *Alfvén and Fälthammer* [1963] considered a low density, kinetic plasma in a simple magnetic mirror field and found that the parallel electric field vanishes if the electrons and ions have the same pitch angle, otherwise charge separation results and an equilibrium electric field is required to ensure the plasma is quasi-neutral along the magnetic flux tube [*Persson*, 1963, 1966]. Following similar treatments many have built upon these seminal works incorporating additional physics. *Alfvén and Fälthammer* [1963] only considered magnetospheric, delta source distributions; *Knight* [1973] relaxed this sim-

plification and included Maxwellian source distributions at both the magnetosphere and the ionosphere. This approach yielded a current-voltage relationship, but did not produce a potential profile, nor did it consider quasi-neutrality. This deficiency was corrected in the models adopted by *Whipple* [1977] and *Chiu and Schulz* [1978]. *Stern* [1981] found that double layers, where the potential varies significantly over a discrete length scale, were a necessary and unavoidable feature of the solutions. *Miller and Khazanov* [1993] produced potential profiles where the source distributions could be manipulated to have a prescribed degree of anisotropy. Others, such as *Vedin and Rönnmark* [2004], have used fluid and fluid-kinetic hybrid models to yield potential distributions and current-voltage relations.

Recently *Boström* [2003, 2004] studied the distribution of current-driven electrostatic potentials along auroral flux tubes analytically, taking into account quasi-neutrality, the kinetic orbital motion of the plasma under the influence of electric and magnetic mirror forces. Paying careful attention to particle accessibility, Boström calculated a series of potential profiles that included potential jumps (double layers), where a significant fraction of the total potential drop along the flux tube occurs over a small length scale comparable to the Debye length. The altitude of the potential jump is sensitive to the relative density and temperature of the source ionospheric and magnetospheric populations. The purpose of this paper is to extend the work of *Boström* [2003, 2004] to investigate how the quasi-neutral electric potential variation is balanced and maintained by the plasma, specifically the electrons, along the flux tube. We derive the moments of the gyrotropic Vlasov equation in order to ascertain what are the significant contributions to the parallel electric field. We also resolve the ambipolar nature of the ionospheric plasma.

This paper is structured as follows: Section 2 sets up the kinetic framework that we will use throughout this paper. It follows the treatment of *Boström* [2003, 2004], briefly summarising the important results relevant for the subsequent work. Sections 3 and 4 build on this by deriving the moments of the gyrotropic Vlasov equation in order to understand how the plasma, specifically the electrons, behave under the influence of the electrostatic potential, the magnetic inhomogeneity and pressure effects.

2. Upward field-aligned current model

Field-aligned currents and their associated parallel electric fields connect the ionosphere to the magnetosphere. Plasma, of both ionospheric and magnetospheric origin, that contributes to the current must have sufficient energy parallel to the ambient magnetic field to overcome electrostatic and magnetic mirror forces. In the absence of a driving electric field, the conservation of the first adiabatic invariant solely dictates the plasma dynamics and determines what population of the given source distributions mirror or precipitate, hence determining the current (termed the thermal current). If the drawn current is larger, then a sympathetic potential drop is required, widening the effective source cone and altering the fraction of potential current carriers. It is desirable to know how such a potential drop is distributed along the flux tube and what controls this variation.

By considering the motion of the ionospheric and magnetospheric plasma, under the influence of a background electromagnetic field, one can obtain a quasi-steady state electric field distribution along the magnetic field while preserving quasi-neutrality. Following Boström's approach [*Boström*, 2003, 2004], we consider a flux tube segment of the global circuitry network surrounding the Earth, with one end grounded in the F region of the ionosphere, the other in the magnetosphere. We assume: (1) a prescribed current density

along the flux tube (or equivalently a prescribed potential drop, ϕ_M); (2) some plasma processes continuously replenish plasma at the ionospheric and magnetospheric ends of the flux tube, with a Maxwell-Boltzmann distribution function; (3) a dynamical equilibrium prevails, where there are no temporal variations; (4) the particles carrying the current along the flux tube are sourced from the distributions that enter/exit at either end of the flux tube; and (5) the plasma responds to electrostatic and magnetic mirror forces.

Within a kinetic framework, the plasma species (α) is described by a distribution function $f_\alpha(W_\parallel, W_\perp, \zeta, U(\zeta))$ where: $W_{\parallel,\perp} = u^2_{\parallel,\perp}/2$ is the non-dimensional kinetic energy component parallel (perpendicular) to the magnetic field; $u_{\parallel,\perp} = v_{\parallel,\perp}(k_B T_M/m)^{-1/2}$ is the corresponding non-dimensional velocity components; T_M is the magnetospheric source temperature; $U = e\phi/(k_B T_M)$ is the normalised electrostatic potential with $U = 0$ at the ionosphere and $U = U_M$ at the magnetospheric end of the flux tube; and $\zeta = B_I/B$ is a field-aligned coordinate normalised by the magnetic flux density at the ionospheric end of the flux tube B_I. Thus, the ionospheric end of the flux tube is at $\zeta = 1$ and the magnetospheric end is $\zeta_M = B_I/B_M$. Note that for ionospheric species, quantities are normalised with respect to the ionospheric source temperature T_I and are denoted with a tilde. Please refer to Appendix A for further details regarding corresponding dimensionalised quantities. The magnetospheric and ionospheric source plasmas are composed of hydrogen and singly-ionised oxygen respectively, characterised by $\tau = T_I/T_M$ and $\nu = n_I/n_M$ which defines their relative temperature and number density. In this study we use $\tau = 1 \times 10^{-3}$ and $\nu = 3 \times 10^3$.

The dynamical evolution of f in phase space is described by the Vlasov equation which can be conveniently solved using Liouville's theorem (i.e. the phase space density, f,

is constant along a particle trajectory). Hence, given a source distribution at ζ_s and knowledge of how the trajectories behave under the influence of external forces, then one can obtain the distribution function at an arbitrary point in space ζ. For a plasma under the influence of electrostatic and magnetic mirror forces, the particle trajectories are described by the following equations of motion

$$W_{\parallel s} + W_{\perp s} \pm U_s = W_{\parallel}(\zeta) + W_{\perp}(\zeta) \pm U(\zeta) \quad (1)$$

$$\zeta_s W_{\perp s} = \zeta W_{\perp}(\zeta) \quad (2)$$

where the plus (minus) sign refers to ions (electrons), for ionospheric species add a tilde. The first equation is the conservation of particle energy and the second represents conservation of the first adiabatic invariant $\mu = \frac{1}{2}mv_{\perp}^2/B$. Using equations (1) and (2) we can determine the populated regions of phase space at an arbitrary point ζ. Particles originating from the source at ζ_s, will occupy the region at ζ defined by

$$W_{\parallel} \geq (\zeta/\zeta_s - 1)W_{\perp} \mp (U - U_s)$$

$$W_{\parallel} \geq 0 \quad (3)$$

The boundaries of these regions will be denoted by Γ_b and Γ_a respectively. The particles satisfying the above conditions that are subsequently lost at the end of the flux tube at ζ_c are given by

$$W_{\parallel} \geq (\zeta/\zeta_c - 1)W_{\perp} \mp (U - U_c) \quad (4)$$

This boundary will be referred to as Γ_c. These boundaries define which particles precipitate and those which mirror. To obtain the potential distribution along the flux tube $U(\zeta)$ the boundaries in phase space of both ion and electron populations must be considered. Figure 1 shows the boundary limits for the magnetospheric and ionospheric electrons only

(for the full set of phase space diagrams, including ions, see *Boström* [2004]). Although we map the ions also, we do not present a detailed discussion of them here, as it is done in *Boström* [2004]. We focus our discussion on the electrons, as the remainder of the paper aims to provide a comparison with studies that consider electron observations. Regions A_1 and A_5 are populated by particles that are lost at the end of the flux tube; regions A_2 and A_6 are populated by particles being mirrored. In reality, particles that are trapped between the magnetic mirror and electrostatic forces constitute an additional population (region A_8 in figure 1) important to the potential distribution. A correct treatment of the trapped population is rather involved; to simplify matters here we do not include a trapped population in our calculations. As demonstrated in figure 10(d) of *Boström* [2004], when no trapped particles are incorporated the potential jump occurs at slightly higher altitudes and accounts for a slightly larger fraction of the total potential jump.

With knowledge of how the distribution functions evolve with position along the flux tube one can easily obtain any bulk commodity at ζ (such as the number density or the fluid velocity) by integrating the distribution function over the appropriate regions in phase space. Summing over the charge densities of the participating plasma species (ions and electrons) yields the total (dimensionless) charge density $\rho(\zeta, U)$. Maps of ρ as a function of ζ and U can be constructed (see Figures 8 and 9 in *Boström* [2004]) that show two distinct regions of positive and negative charge density separated by the contour $\rho = 0$. To obtain the potential distribution along the flux tube, quasi-neutrality is invoked by finding the root $U(\zeta)$ that satisfies $\rho(\zeta, U) = 0$. In general the resulting potential distribution is a multi-valued function of ζ, with no acceptable continuous solution joining the ionosphere to the magnetosphere. This issue can be circumvented by means

of a potential jump (double layer). The maps of ρ apply within the potential jump where ζ is approximately constant and the charge density is only a function of U. The location of the potential jump is found by considering Poisson's equation within the double layer. Following *Boström* [2004] and others [*Langmuir*, 1929; *Stern*, 1981; *Block*, 1972] multiplying Poisson's equation by $\mathrm{d}U/\mathrm{d}\zeta$ and integrating once yields the necessary criteria for the position (ζ_j) of the jump,

$$\int_{U_{j1}}^{U_{j2}} \rho(\zeta_j, U)\mathrm{d}U = \frac{k^2}{2}\left[\left(\frac{\mathrm{d}U}{\mathrm{d}\zeta}\right)_{j1}^2 - \left(\frac{\mathrm{d}U}{\mathrm{d}\zeta}\right)_{j2}^2\right] \approx 0 \tag{5}$$

where $k = \lambda_D \mathrm{d}\zeta/dz$ (approximately constant within the double layer); λ_D is the Debye length; and z is the dimensional coordinate along the flux tube. If the scale of the background magnetic field variation is $\sim R_E$, then $k \approx \lambda_D/R_E \ll 1$. As described by *Stern* [1981] and *Boström* [2004], if $E_\parallel$ adjacent to the jump is much less than that inside, the integral inside equation (5) is zero to leading order.

Note that *Boström* [2004] assumes no potential drop between the jump location and the ionospheric end (i.e. $U_{j1} = 0$). Our calculation relaxes this simplifying assumption, and resolves the ambipolar structure of the ionospheric plasma.

Given the potential variation $U(\zeta)$, the magnetospheric and ionospheric source distribution functions, and the electron trajectories in phase space, we can calculate the moments of the governing Vlasov equation and ascertain how the parallel electric field is maintained, establishing a dynamical equilibrium. An alternative way of expressing this is that we identify the principal routes through which the electric field modifies the electron motion such that a net charge density is established which satisfies Poisson's equation, or quasi-neutrality, as appropriate. For example, the main effect of the electric field could

be to accelerate the current carrying electrons, or to redistribute the mirroring electrons, etc.

3. Parallel electric field

In this section we derive the moments of the Vlasov equation. Initially, we will suppress the non-dimensional notation to aid a physical appreciation.

3.1. Derivation of electron fluid equations

Assuming the plasma to be collisionless and the guiding centre approximation valid, the electrons are described by a gyrotropic distribution function $f = f(l, v_\parallel, v_\perp, t)$ which is a function of the distance along the flux tube, l; the parallel guiding centre velocity, $v_\parallel$; the perpendicular speed of the electrons, $v_\perp$; and time, t. Under the influence of a parallel electric field and the magnetic mirror force, the electron dynamics are described by $m\mathrm{d}v_\parallel/\mathrm{d}t = -eE_\parallel - \mu\partial B/\partial l$, where μ is the first adiabatic invariant. In the steady state $f = f(l, v_\parallel, v_\perp)$ and the gyrotropic Vlasov equation becomes

$$v_\parallel \frac{\partial f}{\partial \ell} - \left(\frac{eE_\parallel}{m} + \frac{v_\perp^2}{2B}\frac{\partial B}{\partial \ell} \right) \frac{\partial f}{\partial v_\parallel} + \frac{v_\parallel v_\perp}{2B}\frac{\partial B}{\partial \ell}\frac{\partial f}{\partial v_\perp} = 0 \tag{6}$$

where $f = f_M + f_I$, and f_M and f_I represent the magnetospheric and ionospheric electron distribution functions respectively. The average, macroscopic description of the plasma is found by calculating the moments of the Vlasov equation. Taking the zeroth moment yields the continuity equation

$$\frac{\partial}{\partial \ell}\left(n\bar{v}_\parallel\right) - \frac{n\bar{v}_\parallel}{B}\frac{\partial B}{\partial \ell} = 0, \tag{7}$$

where $\bar{v}_\parallel = \int v_\parallel f \mathrm{d}\mathbf{v}/n$ and $n = \int f \mathrm{d}\mathbf{v}$. Noting that $j_\parallel = \pm en\bar{v}_\parallel$, this can be rewritten to explicitly emphasize that $j_\parallel/B$ is conserved along a flux tube,

$$\frac{\partial}{\partial \ell}\left(\frac{j_\parallel}{B}\right) = 0, \tag{8}$$

This expression provides a useful means of calculating $\bar{v}_\parallel$ along the flux tube. Calculating the first moment, by multiplying the Vlasov equation by $mv_\parallel$ and integrating over velocity space, gives the momentum equation

$$\begin{aligned} -\frac{en}{m}E_\parallel \;=\; & \frac{\partial}{\partial \ell}\int v_\parallel^2 f \mathrm{d}\mathbf{v} + \frac{1}{2B}\frac{\partial B}{\partial \ell}\int v_\perp^2 f \mathrm{d}\mathbf{v} \\ & -\frac{1}{B}\frac{\partial B}{\partial \ell}\int v_\parallel^2 f \mathrm{d}\mathbf{v} \end{aligned} \tag{9}$$

where use is made of equation (7). This equation can be recast in terms of the parallel ($p_\parallel$) and perpendicular ($p_\perp$) electron pressure

$$E_\parallel = -\frac{1}{en}\left(\frac{\partial p_\parallel}{\partial \ell} + mn\bar{v}_\parallel\frac{\partial \bar{v}_\parallel}{\partial \ell} + \frac{p_\perp - p_\parallel}{B}\frac{\partial B}{\partial \ell}\right) \tag{10}$$

where the parallel pressure is

$$p_\parallel = nm\left(\int v_\parallel^2 f \mathrm{d}\mathbf{v} - \bar{v}_\parallel^2\right) \tag{11}$$

and the perpendicular pressure

$$p_\perp = \frac{m}{2}\int v_\perp^2 f \mathrm{d}\mathbf{v} \tag{12}$$

Equation (10) clearly exhibits the main components balancing the parallel electric field: the first term is the parallel pressure force; the second term is a measure of the electron fluid acceleration; and the third term quantifies the effect of the magnetic inhomogeneity: $(p_\perp/B)\partial B/\partial l$ is the magnetic mirror force and $-(p_\parallel/B)\partial B/\partial l$ is the pressure force associated with the changing cross-sectional area of the flux tube – note that these two forces are in opposition [*Comfort*, 1988].

Rewriting the problem in non-dimensional form yields

$$\begin{aligned}\bar{E}_\parallel &= \frac{1}{N}\left(\frac{\partial \bar{p}_\parallel^{\mathrm{mag}}}{\partial y} + N\bar{u}_\parallel\frac{\partial \bar{u}_\parallel}{\partial y} + \frac{\bar{p}_\parallel^{\mathrm{mag}} - \bar{p}_\perp^{\mathrm{mag}}}{\zeta}\frac{\partial \zeta}{\partial y}\right) \\ &\quad + \frac{\tau}{N}\left(\frac{\partial \bar{p}_\parallel^{\mathrm{iono}}}{\partial y} + \frac{\bar{p}_\parallel^{\mathrm{iono}} - \bar{p}_\perp^{\mathrm{iono}}}{\zeta}\frac{\partial \zeta}{\partial y}\right) \\ &= \bar{E}_\parallel^{\mathrm{mag}} + \bar{E}_\parallel^{\mathrm{iono}} \end{aligned} \tag{13}$$

where

$$\bar{E}_\parallel = eR_E E_\parallel/(k_B T_M) \tag{14}$$

$$\bar{p}_{\parallel,\perp}^{\mathrm{mag}} = p_{\parallel,\perp}^{\mathrm{mag}}/(k_B T_M n_0) \tag{15}$$

$$\bar{p}_{\parallel,\perp}^{\mathrm{iono}} = p_{\parallel,\perp}^{\mathrm{iono}}/(k_B T_I n_0) \tag{16}$$

$$N = n/n_0 \tag{17}$$

$$\bar{f}_M = f_M(k_B T_M/m)^{3/2}/n_0 \tag{18}$$

$$\bar{f}_I = f_I(k_B T_I/m)^{3/2}/n_0 \tag{19}$$

and we have performed the change of variable to a field-aligned coordinate $y = (l_m - l)/R_E$ which is measured from the ionospheric end, such that $y = 0$ is the base of the F region and y increases as we approach the magnetosphere. Further details regarding dimensionalised quantities are given in Appendix A. The magnetospheric electron contribution can be

decomposed into that from the precipitating and mirroring populations: $\bar{p}_{\|}^{\mathrm{mag}} = \bar{p}_{\|}^{\mathrm{mag,p}} + \bar{p}_{\|}^{\mathrm{mag,m}}$ and $\bar{p}_{\perp}^{\mathrm{mag}} = \bar{p}_{\perp}^{\mathrm{mag,p}} + \bar{p}_{\perp}^{\mathrm{mag,m}}$ such that $\bar{E}_{\|}^{\mathrm{mag}} = \bar{E}_{\|}^{\mathrm{mag,p}} + \bar{E}_{\|}^{\mathrm{mag,m}}$, where

$$\bar{p}_{\|}^{\mathrm{mag,p}} = \int_{A_1} u_{\|}^2 \bar{f}_M \mathrm{d}\mathbf{u} - N\bar{u}_{\|}^2 \tag{20}$$

$$\bar{p}_{\|}^{\mathrm{mag,m}} = \int_{2A_2} u_{\|}^2 \bar{f}_M \mathrm{d}\mathbf{u} \tag{21}$$

$$\bar{p}_{\perp}^{mag,p} = \int_{A_1} u_{\perp}^2 \bar{f}_M \mathrm{d}\mathbf{u} \tag{22}$$

$$\bar{p}_{\perp}^{mag,m} = \int_{2A_2} u_{\perp}^2 \bar{f}_M \mathrm{d}\mathbf{u} \tag{23}$$

and

$$\bar{u}_{\|} = \frac{\zeta_M}{N\zeta} \int_{\mathrm{source}} u_{\|} \bar{f}_M \mathrm{d}\mathbf{u} \tag{24}$$

The latter expression is a convenient way of calculating $\bar{u}_{\|}$ along the flux tube exploiting the conservation of $i_{\|}\zeta$ ($i_{\|}$ being the dimensionless current density $j_{\|}$). A similar relation can be used for the ionospheric electrons. In this notation the ionospheric electron pressure becomes

$$\bar{p}_{\|}^{\mathrm{iono}} = \int_{A_5+2A_6} \tilde{u}_{\|}^2 \bar{f}_I \mathrm{d}\mathbf{u} - N\bar{u}_{\|}^2 \tag{25}$$

$$\bar{p}_{\perp}^{\mathrm{iono}} = \int_{A_5+2A_6} \tilde{u}_{\perp}^2 \bar{f}_I \mathrm{d}\tilde{\mathbf{u}} \tag{26}$$

Evaluating the integrals over the appropriate regions of phase space defined by equations (3) and (4) we can calculate the contributions to the parallel electric field $\bar{E}_{\|}$.

When a potential jump occurs it is also of interest to analyse how the parallel electric field within the jump is balanced by the electrons. A full, self-consistent calculation for the electric field in this region would require explicitly solving Poisson's equation, since we would be working on a length scale where quasi-neutrality breaks down. Here, we probe the plasma behaviour by prescribing a electric potential (consistent with U_{j1} and

U_{j2}) within the double layer to get a glimpse of the electron behaviour. Ultimately a self-consistent calculation is required. Within the potential jump we choose a dimensionless length scale of interest Λ ($= (l_m - l)/R_0$, where R_0 is expected to be of the order of the Debye length) that is sufficiently small such that there is no significant spatial variation in the magnetic field $\partial\zeta/\partial\Lambda \approx 0$, yet acceptably large that there is a spatial variation in the distribution function. On such a length scale any forces associated with the ambient magnetic inhomogeneity are negligible, therefore

$$\kappa\bar{E}_\parallel = \frac{1}{N}\left(\frac{\partial\bar{p}_\parallel^{\rm mag}}{\partial\Lambda} + N\bar{u}_\parallel\frac{\partial\bar{u}_\parallel}{\partial\Lambda}\right) + \frac{\tau}{N}\frac{\partial\bar{p}_\parallel^{\rm iono}}{\partial\Lambda} \tag{27}$$

where $\kappa = R_0/R_E$.

4. Contributions to the parallel electric field $\bar{E}_\parallel$

Given the potential variation $U(\zeta)$ there are two equivalent and complementary methods for calculating the parallel electric field $\bar{E}_\parallel$. The simplest and most direct involves calculating the derivative of the normalised potential variation with respect to y, $\bar{E}_\parallel = \partial U/\partial y$. In the analysis presented here, given $U(\zeta)$: the magnetospheric and ionospheric source distributions, and the electron trajectories in phase space, we can calculate the moments of the Vlasov equation to find $\bar{E}_\parallel$. In doing so, we gain the added benefit of understanding what balances the parallel electric field and how it is maintained. The contributions to $\bar{E}_\parallel$ calculated from equation (13) is equal to $\bar{E}_\parallel = \partial U/\partial y$ (the alternative method) and agrees to $O(10^{-5})$ – this is an important confirmation of the calculations presented here.

Following Boström's model (as described in section 2), the variation of the electric potential as a function of y along the flux tube is shown in Figures 2 and 3. For this particular

calculation the prescribed potential drop was $U_M = -10$ ($j_{\|I} \approx 2.7\times10^{-12} n_e^M \sqrt{T_e^M}$ Am^{-2}, for $n_e^M = 10^6$ m^{-3} and $k_B T_e^M = 500$eV, $j_{\|I} \approx 6.5\mu$Am^{-2}, which corresponds to $\phi_M = 5$ kV) and the key dimensionless parameters listed in table 1 were used. The potential jump was found (using Equation 5) to occur at $\zeta_j = 13.47$ (which occurs at a radial distance $2.33R_E$ from the Earth), where the potential changes suddenly from $U_{j1} = -2.31 \times 10^{-3}$ to $U_{j2} = -8.53$. Figure 2 exhibits the potential variation along the entire flux tube under consideration, showing the three main regions of interest: earthward of the potential jump (pre-potential jump); within the potential jump; and the magnetospheric end of the jump (post-potential jump). Note that the potential variation in the pre-jump region and within the potential jump varies on a scale unresolved by the plot. Figure 3 shows the detail of the potential variation and the variation of the parallel electric field within the three regions. Note that within the potential jump the plotted parallel electric field is $\kappa\bar{E}_\|$ where $\kappa = R_0/R_E$, and R_0 is the field-aligned scale of the jump.

To aid in a physical appreciation of the plots we shall set $n_e^M = 10^6$ m^{-3}, $k_B T_e^M = 500$eV and the spatial extent of the double layer to ≈ 100 km. The pre-jump region then occurs over a length scale $\approx$ 8900 km, where the potential difference $\Delta\phi \approx 1.25$ V and the peak electric field $|E_\|^{peak}| \approx 62.7$ μVm^{-1}; within the potential jump $\Delta\phi \approx 4.264$ kV and $|E_\|^{peak}| \approx 320$ mVm^{-1}; and in the post-jump region $\Delta\phi \approx 735$ V and $|E_\|^{peak}| \approx 0.3$ mVm^{-1} over a spatial range of $\approx$ 48000 km. These values are in general agreement with *Ergun et al.* [2002b] and *Ergun et al.* [2004].

In figure 4 we show the total space charge distribution within the potential jump, which integrated over U is zero, consistent with equation (5). Within the jump, a tanh potential

variation is used, which closely mimics a typical sheath field, such that the electric field at the edges of the double layer is zero.

Figures 5 and 6 show the electron number density as a function of y, decomposed into contributions from the ionospheric (N_e^I) and magnetospheric (N_e^M) species; the magnetospheric mirroring ($N_e^{M,m}$) and precipitating populations ($N_e^{M,p}$) respectively. In the pre-potential jump region (i.e. earthward of the jump), there is a pronounced peak in N_e^M resulting from a combination of competing effects acting on the magnetospheric electrons; Moving Earthwards $\bar{E}_\parallel$ (the magnetic mirror force) tends to accelerate (decelerate) the magnetospheric electrons. Additionally, as the magnetic flux density increases, the cross-sectional area of the flux tube decreases. As the ionosphere is approached, the precipitating electron population (and the empty region in phase space associated with them not mirroring) grows in significance as fewer electrons are mirrored leading to a decline in the density. This effect is evident in the pre-jump region in figures 5 and 6.

The effect of the magnetic mirror force is clearly exhibited in the magnetospheric pressure components in Figure 7: as the magnetospheric electrons move from the source, the magnetic anisotropy gradually increases and the mirror force grows increasingly prominent. Conservation of the first adiabatic invariant transfers energy from the particles parallel motion to its perpendicular motion increasing $\bar{p}_\perp^{\text{mag}}$, hence $\bar{p}_\perp^{\text{mag}} > \bar{p}_\parallel^{\text{mag}}$.

Similar competing effects dictate the dynamics and hence the density variation of N_e^I (see Figure 5). Under the sole influence of an upward electric field, ionospheric electrons with a non-zero source temperature would be expected to be restricted to the ionosphere, and have a density variation $\propto \nu \exp(-\tilde{U})$, where $\tilde{U} = U/\tau$. However, the combined competing effects introduced via the magnetic inhomogeneity complicates this simple

dependence. The magnetic mirror force aids in allowing the electrons to reach further along the flux tube than would be possible without it, whereas the pressure force associated with the changing cross-sectional area of the flux tube, acts to constrain the electrons close to the ionosphere. Within the potential jump, where forces associated with the magnetic inhomogeneity are negligible and U varies dramatically, the ionospheric electrons are excluded and N_e^I tends to zero. The effect of the magnetic mirror force is evident in the behaviour of the parallel and perpendicular ionospheric pressure terms (Figure 8): moving away from the ionosphere, conservation of magnetic moment converts $u_\perp$ to $u_\parallel$, causing the distribution to become highly collimated and having $\bar{p}_\parallel^{\text{iono}} > \bar{p}_\perp^{\text{iono}}$. The exclusion of these electrons from traversing the potential jump means $\bar{p}_\parallel^{\text{iono}}$ and $\bar{p}_\perp^{\text{iono}}$ are negligible post-jump and throughout most of the jump.

Using the expressions derived in section 3 and the solution for $U(\zeta)$ obtained from Boström's model, we can now analyse how the electric field is balanced and maintained by the electrons. Contributions from the precipitating, mirroring and ionospheric electron populations in the three regions of interest are shown in figure 9, which are plotted normalised to the total parallel electric field $\bar{E}_\parallel$ at each value of y (or Λ). In the pre-potential jump region the ionospheric population supports virtually the entire electric field close to the earth due to $N_e^I \gg N_e^M$. When N_e^I becomes comparable to N_e^M (at $\Lambda \approx -4$, see Figure 5) the influence of the ionospheric population diminishes and the magnetospheric population becomes the primary contributor to $\bar{E}_\parallel$. Of this species it is the mirroring population ($N_e^{M,m}$) that balances the majority of $\bar{E}_\parallel$ due to it's greater number density relative to the precipitating particles (Figure 6). This trend continues in the post-potential jump region: $|\bar{E}_\parallel^{\text{mag,m}}| > |\bar{E}_\parallel^{\text{mag,p}}|$ and their respective spatial variations within and outwith the

potential jump region correlate with those of $N_e^{M,m}$ and $N_e^{M,p}$ (Figure 6). Although the precipitating electrons carry the field-aligned current it is the mirroring population that actually balances the majority of $\bar{E}_\parallel$ which accelerates the precipitating electrons. This result underlines the importance of the mirroring electron population, as they play the dominant role in maintaining the quasi-neutrality of the system.

In this system, the electron guiding centre dynamics are dictated by the electric force, the pressure force and the forces associated with the magnetic inhomogeneity. Figure 10 exhibits how these forces acting on the ionospheric electrons balance the parallel electric field in the pre-jump region. Close to the ionosphere, the electrons thermal energy exceeds its potential energy ($|\tilde{U}(y < 0.05)| < 1$), as a result thermal effects (the parallel pressure gradient) locally support $\bar{E}_\parallel$. As y increases and the electrons are decelerated through a growing electric potential ($|\tilde{U}(y < 0.05)| > 1$), thermal effects diminish leaving those associated with the magnetic inhomogeneity to dominate. Now, the parallel pressure gradient and the competing parallel pressure force associated with the magnetic inhomogeneity largely cancel each other leaving the magnetic mirror force as the main effect balancing the majority of $\bar{E}_\parallel$.

Within the potential jump (Figure 11), the main contributor balancing $\bar{E}_\parallel$ changes suddenly from the ionospheric to the magnetospheric species since N_e^I falls to almost zero. The small length scale of the transition means the magnetospheric parallel pressure gradient dominates the mirror force, and balances the parallel electric field.

In the post-jump region, where the magnetospheric species dominates, it is their parallel pressure gradient that balances the majority of the parallel electric field (Figure 12). Additionally, the electric potential energy of the electrons is less than their thermal energy

($U < 1$), highlighting the importance of thermal effects in this region. At $y \approx 3$ the magnetic inhomogeneity is approximately equal in magnitude to the parallel pressure force; as y decreases, both increase in magnitude with the latter becoming the dominant effect. We note some details of the magnetic inhomogeneity term, $(\bar{p}_{\parallel}^{mag} - \bar{p}_{\perp}^{mag})(\partial\zeta/\partial y)/(N\zeta)$: In a trapped, perfectly mirroring isotropic Maxwellian distribution, there would be no current and $p_{\parallel}$ and $p_{\perp}$ would have the same (constant) value along the entire field line. The individual contributions of $p_{\parallel}$ and $p_{\perp}$ to the above term are not zero, but are equal and opposite such that they cancel and yield the solution $\bar{E}_{\parallel} = 0$. The current carrying case we present in Figure 12, seems to be a perturbation to this state, inasmuch as the contributions of $p_{\parallel}$ and $p_{\perp}$ to the above term are a factor of $O(10)$ greater than the sum of the contributions. Thus the magnetic inhomogeneity term only plays a secondary role in accounting for $\bar{E}_{\parallel}$ in the magnetosphere.

5. Discussion and Conclusion

In this paper we have studied the contributions to the parallel electric field responsible for coupling the ionosphere to the magnetosphere. Following Boström's kinetic model [*Boström*, 2003, 2004] we considered the motion of the ionospheric and magnetospheric plasma under the influence of electrostatic and magnetic mirror forces, to obtain how the quasi-neutral electric potential varies with position along the flux tube $U(\zeta)$. Invariably we find that $U(\zeta)$ contains a jump which may correspond to a double layer where the electric potential suddenly jumps over a length scale comparable to the Debye length. The potential jump splits $U(\zeta)$ into three distinct regions: the region earthward of the potential jump (pre-jump); within the potential jump; and the magnetospheric side of the potential jump (post-jump). This is in qualitative agreement with the model of

parallel electric fields proposed by *Mozer and Hull* [2001] and the numerical simulations by *Ergun et al.* [2000]. In the later, multiple transition layers (double layers) can occur depending on the specific conditions invoked at the ionospheric boundary. However, our results differ with *Ergun et al.* [2002b, 2004] who reported that $\approx 10\%$ of the total auroral potential is concentrated in the double layer. The difference can be attributed to the relative complexity of the models involved. *Ergun et al.* [2002b, 2004] consider a more complex system incorporating a greater number of particle species including a trapped population, which we neglect. The inclusion of extra particle species can give rise to more than one jump in the potential, whilst the inclusion of a trapped population (Figure 10(d) in *Boström* [2004]) can reduce the potential drop we find in figure 2 by $\approx 50\%$, and lower the altitude of the jump by $\approx 20\%$. The remainder of the potential is then dropped gradually over the magnetospheric portion of the field line. Evidently the details of the potential solution are sensitive to the particle species that are present.

With the variation $U(\zeta)$, we evaluated the moments of the governing gyrotropic Vlasov equation to study how the quasi-neutral electric field $\bar{E}_{\parallel}$ is balanced and maintained by the electrons in each of these three regions. Our results show that in the pre-jump region the ionospheric species supports the electric field as a consequence of $N_e^I \gg N_e^M$. Close to the ionosphere it is the parallel pressure gradient that locally balances $\bar{E}_{\parallel}$, but as we approach the potential jump and the electrons are decelerated by the electric field, the magnetic mirror force becomes the main contributor to $\bar{E}_{\parallel}$. Within the potential jump itself, as N_e^I falls to zero, the magnetospheric electrons become the sole species maintaining $\bar{E}_{\parallel}$ through the parallel pressure gradient. This is consistent with Polar [*Hull et al.*, 2003a, b] and FAST [*Chaston et al.*, 2007] observations, where detailed analysis of

large-amplitude electric field structures (double layers) suggest that they are balanced by ambipolar effects. In the post-jump region, as we approach the magnetosphere, it is the magnetospheric parallel pressure gradient that supports the majority of $\bar{E}_{\parallel}$. Additionally, we found that although the precipitating electrons carry the field-aligned current it is the mirroring population that actually balances the majority of $\bar{E}_{\parallel}$ which accelerates the precipitating population. The mirroring population, being more abundant, is crucial for quasi-neutrality considerations.

Related studies by Vedin and Rönnmark [*Vedin and Rönnmark*, 2005, 2006, 2007] find the main contribution to the parallel electric field is from thermal effects consistent with *Hull et al.* [2003a, b] and in general agreement with our calculations within the potential jump and in the post-jump region. In general the contribution from the magnetic inhomogeneity is comparatively smaller but still significant [*Vedin and Rönnmark*, 2005] - this is echoed in our post-jump calculations, particularly as the outer magnetosphere is approached. Inertial effects [*Rönnmark*, 1999; *Wright et al.*, 2002; *Wright and Hood*, 2003] have also been suggested as an important contributor to the electric field. In a cold plasma [*Wright and Hood*, 2003], electron inertia must dominate $\bar{E}_{\parallel}$; for a warmer plasma, such as in Earth's magnetosphere, our results show that it is no longer dominant. Previously the role of $\bar{E}_{\parallel}$ and U in overcoming the mirror force experienced by precipitating magnetospheric electrons has been stressed. Whilst this is still an accurate statement, in this paper we have shown that it is the more plentiful electrons, that do not contribute to the current, that are responsible for the variation of U along the field line, and hence determine where electron acceleration occurs.

Appendix A: Table of quantities

Appendix B: Calculation of pressure terms

B1. Magnetospheric electrons

For the magnetospheric electrons the relevant integrals are evaluated over the appropriate areas in Figure 1. Firstly the parallel pressure,

$$\begin{aligned}\int\limits_{A_1+2A_2} u_\parallel^2 \bar{f}_M \mathrm{d}\mathbf{u} &= \int\limits_{A_1+A_2} u_\parallel^2 \bar{f}_M \mathrm{d}\mathbf{u} + \int\limits_{A_2} u_\parallel^2 \bar{f}_M \mathrm{d}\mathbf{u} \\ &= \eta_1 + \eta_2 \end{aligned} \tag{B1}$$

where

$$\begin{aligned}\eta_1 &= \int\limits_{W_\parallel=0}^{\infty}\int\limits_{W_\perp=0}^{\infty} u_\parallel^2 \bar{f}_M \mathrm{d}\mathbf{u} - \int\limits_{W_\parallel=0}^{U-U_M}\int\limits_{W_\perp=0}^{\frac{W_\parallel-U+U_M}{\zeta/\zeta_M-1}} u_\parallel^2 \bar{f}_M \mathrm{d}\mathbf{u} \\ &= \frac{e^{U-U_M}}{2}\mathrm{erfc}\left(\sqrt{U-U_M}\right) - \frac{s^{-3/2}}{\sqrt{\pi}}\mathrm{D}\left(\sqrt{s(U-U_M)}\right) \\ &\quad + \frac{\zeta_M}{\zeta}\sqrt{\frac{U-U_M}{\pi}} \end{aligned} \tag{B2}$$

where $D(x)$ is Dawson's Integral, and

$$\begin{aligned}\eta_2 &= \int\limits_{W_\parallel=0}^{U-U_D}\int\limits_{W_\perp=\frac{W_\parallel-U+U_M}{\zeta/\zeta_M-1}}^{\infty} u_\parallel^2 \bar{f}_M \mathrm{d}\mathbf{u} \\ &\quad + \int\limits_{W_\parallel=U-U_D}^{\infty}\int\limits_{W_\perp=\frac{W_\parallel-U}{\zeta-1}}^{\infty} u_\parallel^2 \bar{f}_M \mathrm{d}\mathbf{u} \\ &= e^{-k}\left[\left(\frac{\zeta_M-1}{\zeta}\right)\sqrt{\frac{U-U_D}{\pi}}\right.\end{aligned}$$

$$+\frac{t}{2}^{-3/2} e^{t(U-U_D)}\mathrm{erfc}\left(\sqrt{t(U-U_D)}\right)$$
$$-\frac{s^{-3/2}}{\sqrt{\pi}} D\left(\sqrt{s(U-U_D)}\right)\Big] \tag{B3}$$

where $s = \zeta/(\zeta_M - \zeta)$, $t = \zeta/(\zeta - 1)$ and $U_D = (1 - 1/\zeta)U_M/(1 - 1/\zeta_M)$. The contribution from the precipitating electrons is given by

$$\bar{p}_{\parallel}^{\mathrm{mag,p}} = \int_{A_1} u_{\parallel}^2 \bar{f}_M \mathrm{d}\mathbf{u} - N\bar{u}_{\parallel}^2 = \eta_1 - \eta_2 \tag{B4}$$

and the contribution from the mirroring electrons is

$$\bar{p}_{\parallel}^{\mathrm{mag,m}} = \int_{2A_2} u_{\parallel}^2 \bar{f}_M \mathrm{d}\mathbf{u} = 2\eta_2 \tag{B5}$$

Secondly, the perpendicular pressure

$$\begin{aligned}\int_{A_1+2A_2} u_{\perp}^2 \bar{f}_M \mathrm{d}\mathbf{u} &= \int_{A_1+A_2} u_{\perp}^2 \bar{f}_M \mathrm{d}\mathbf{u} + \int_{A_2} u_{\perp}^2 \bar{f}_M \mathrm{d}\mathbf{u} \\ &= \mu_1 + \mu_2\end{aligned} \tag{B6}$$

where

$$\begin{aligned}\mu_1 &= \int_{W_{\parallel}=0}^{\infty}\int_{W_{\perp}=0}^{\infty} u_{\perp}^2 \bar{f}_M \mathrm{d}\mathbf{u} - \int_{W_{\parallel}=0}^{U-U_M}\int_{W_{\perp}=0}^{\frac{W_{\parallel}-U+U_M}{\zeta/\zeta_M-1}} u_{\perp}^2 \bar{f}_M \mathrm{d}\mathbf{u} \\ &= e^{U-U_M}\mathrm{erfc}\left(\sqrt{U-U_M}\right) - \frac{\zeta_M}{\zeta}\sqrt{\frac{U-U_M}{\pi}} \\ &+ \frac{2}{\sqrt{s\pi}}\left(1 + \frac{\zeta_M}{2\zeta} - \frac{U-U_M}{\frac{\zeta}{\zeta_M}-1}\right) \mathrm{D}\left(\sqrt{s(U-U_M)}\right)\end{aligned} \tag{B7}$$

and

$$\begin{aligned}\mu_2 &= \int_{W_\parallel=0}^{U-U_D} \int_{W_\perp=\frac{W_\parallel-U+U_M}{\zeta/\zeta_M-1}}^{\infty} u_\perp^2 \bar{f}_M \mathrm{d}\mathbf{u} \\ &+ \int_{W_\parallel=U-U_D}^{\infty} \int_{W_\perp=\frac{W_\parallel-U}{\zeta-1}}^{\infty} u_\perp^2 \bar{f}_M \mathrm{d}\mathbf{u} \\ &= e^{-k}\left[\left(\frac{1-\zeta_M}{\zeta}\right)\sqrt{\frac{U-U_D}{\pi}}\right. \\ &+ \frac{e^{t(U-U_D)}}{\sqrt{t}}\left(1-\frac{U}{\zeta-1}+\frac{1}{2\zeta}\right)\mathrm{erfc}\left(\sqrt{t(U-U_D)}\right) \\ &+ \frac{2}{\sqrt{s\pi}}\left(1-\frac{U-U_M}{\frac{\zeta}{\zeta_M}-1}+\frac{\zeta_M}{2\zeta}\right) \\ &\left. D\left(\sqrt{s(U-U_D)}\right)\right] \end{aligned} \tag{B8}$$

The contribution from the precipitating electrons is given by

$$\bar{p}_\perp^{mag,p} = \int_{A_1} u_\perp^2 \bar{f}_M \mathrm{d}\mathbf{u} = \mu_1 - \mu_2 \tag{B9}$$

and the contribution from the mirroring electrons is

$$\bar{p}_\perp^{mag,m} = \int_{2A_2} u_\perp^2 \bar{f}_M \mathrm{d}\mathbf{u} = 2\mu_2 \tag{B10}$$

B2. Ionospheric electrons

Following the same mantra we consider the ionospheric electrons. Firstly the parallel pressure

$$\begin{aligned}\int_{A_5+2A_6} \tilde{u}_\parallel^2 \bar{f}_I \mathrm{d}\tilde{\mathbf{u}} &= \int_{2(A_5+A_6)} \tilde{u}_\parallel^2 \bar{f}_I \mathrm{d}\tilde{\mathbf{u}} - \int_{A_5} \tilde{u}_\parallel^2 \bar{f}_I \mathrm{d}\tilde{\mathbf{u}} \\ &= 2\gamma_1 - \gamma_2 \end{aligned} \tag{B11}$$

where

$$\begin{aligned}\gamma_1 &= \int_{\tilde{W}_\parallel=0}^{\infty}\int_{\tilde{W}_\perp=0}^{\frac{\tilde{W}_\parallel-U/\tau}{\zeta-1}} \tilde{u}_\parallel^2 \bar{f}_I \mathrm{d}\tilde{\mathbf{u}} \\ &= \frac{\nu e^{\frac{U}{\tau}}}{2} - \frac{\nu e^{\frac{tU}{\tau}}}{2t^{3/2}}\end{aligned} \tag{B12}$$

Since area A_5 is identical to area A_1 with potentials scaled by τ, γ_2 can be found by substituting $U = U/\tau$, $U_M = U_M/\tau$ and $U_D = U_D/\tau$ into $\eta_1 - \eta_2$ (given in equations (B2) and (B3)) and multiplying by $\nu e^{U_M/\tau}$ due to the difference in $\bar{f}_M$ and $\bar{f}_I$ to give

$$\begin{aligned}\frac{\gamma_2}{\nu} &= \frac{e^{\frac{U}{\tau}}}{2}\mathrm{erfc}\left(\sqrt{\frac{U-U_M}{\tau}}\right) \\ &- \frac{s^{-3/2}}{\sqrt{\pi}} e^{\frac{U_M}{\tau}} \mathrm{D}\left(\sqrt{\frac{s}{\tau}(U-U_M)}\right) + e^{\frac{U_M}{\tau}} \frac{\zeta_M}{\zeta}\sqrt{\frac{U-U_M}{\pi\tau}} \\ &- \left(\frac{\zeta_M - 1}{\zeta}\right) e^{\frac{tU_D}{\tau}} \sqrt{\frac{U-U_D}{\pi\tau}} \\ &- \frac{t^{-3/2}}{2} e^{\frac{tU}{\tau}} \mathrm{erfc}\left(\sqrt{\frac{t}{\tau}(U-U_D)}\right) \\ &+ s^{-3/2} e^{\frac{tU_D}{\tau}} \mathrm{D}\left(\sqrt{\frac{s}{\tau}(U-U_D)}\right)\end{aligned} \tag{B13}$$

The perpendicular pressure is

$$\begin{aligned}\int_{A_5+2A_6} \tilde{u}_\perp^2 \bar{f}_I \mathrm{d}\tilde{\mathbf{u}} &= \int_{2(A_5+A_6)} \tilde{u}_\perp^2 \bar{f}_I \mathrm{d}\tilde{\mathbf{u}} - \int_{A_5} \tilde{u}_\perp^2 \bar{f}_I \mathrm{d}\tilde{\mathbf{u}} \\ &= 2\delta_1 - \delta_2\end{aligned} \tag{B14}$$

where

$$\begin{aligned}\delta_1 &= \int_{\tilde{W}_\parallel=0}^{\infty} \int_{\tilde{W}_\perp=0}^{\frac{\tilde{W}_\parallel - U/\tau}{\zeta-1}} \tilde{u}_\perp^2 \bar{f}_I \mathrm{d}\tilde{\mathbf{u}} \\ &= \nu\left(e^{\frac{U}{\tau}} + \frac{e^{\frac{tU}{\tau}}}{\sqrt{t}}\left(\frac{U/\tau}{\zeta-1} - 1 - \frac{1}{2\zeta}\right)\right) \end{aligned} \tag{B15}$$

As in the parallel integral case, we can find δ_2 simply by substituting $U = U/\tau$, $U_M = U_M/\tau$ and $U_D = U_D/\tau$ into $\mu_1 - \mu_2$ (found in equations (B7) and (B8)), and multiplying the answer by $\nu e^{\frac{U_M}{\tau}}$ to obtain

$$\begin{aligned}\frac{\delta_2}{\nu} &= e^{\frac{U}{\tau}} \mathrm{erfc}\left(\sqrt{\frac{U-U_M}{\tau}}\right) \\ &- \frac{\zeta_M}{\zeta} e^{\frac{U_M}{\tau}} \sqrt{\frac{U-U_M}{\pi\tau}} + \left(\frac{\zeta_M - 1}{\zeta}\right) e^{\frac{tU_D}{\tau}} \sqrt{\frac{U-U_D}{\pi\tau}} \\ &+ \frac{2}{\sqrt{s\pi}}\left(1 + \frac{\zeta_M}{2\zeta} - \frac{U-U_M}{\tau\left(\frac{\zeta}{\zeta_M} - 1\right)}\right) \\ &\left(e^{\frac{U_M}{\tau}} \mathrm{D}\left(\sqrt{\frac{s}{\tau}(U-U_M)}\right)\right. \\ &\left. - e^{\frac{tU_D}{\tau}} \mathrm{D}\left(\sqrt{\frac{s}{\tau}(U-U_D)}\right)\right) \\ &+ \frac{e^{\frac{tU}{\tau}}}{\sqrt{t}}\left(\frac{U}{\tau(\zeta-1)} - 1 - \frac{1}{2\zeta}\right) \\ &\mathrm{erfc}\left(\sqrt{\frac{t}{\tau}(U-U_D)}\right) \end{aligned} \tag{B16}$$

Since the ionospheric temperature is small in comparison to the magnetospheric temperature, the integrals over region A_5 tend to zero and no ionospheric electrons surmount the potential barrier.

Acknowledgments. CRS gratefully acknowledges funding from the UK Science and Technology Funding Council (PP/E001122/1). The authors would like to thank the anonymous referees, whose valuable feedback helped us to improve this manuscript.

References

Alfvén, H., C. G. Fälthammer (1963), *Cosmical Electrodynamics*, 2nd ed., Clarendon, Oxford, UK.

Block, L. P. (1972), Potential double layers in the ionosphere *Cosmic Electrodyn., 3*, 349-376

Boström, R. (2003), Kinetic and space charge control of current flow and voltage drops along magnetic flux tubes: Kinetic effects, *J. Geophys. Res., 108*, A4, 8004 doi:10.1029/2002JA009295.

Boström, R. (2004), Kinetic and space charge control of current flow and voltage drops along magnetic flux tubes: 2. Space charge effects, *J. Geophys. Res., 109*, A01208, doi:10.1029/2003JA010078.

Chaston, C. C., A. J. Hull, J. W. Bonnell, C. W. Carlson, R. E. Ergun, R. J. Strangeway, and J. P. McFadden (2007), Large parallel electric fields, currents, and density cavities in dispersive Alfvén waves above the aurora, *J. Geophys. Res., 112*,A05215, doi:10.1029/2006JA012007.

Chiu, Y. T. and M. Schulz (1978), Self-consistent particle and parallel electrostatic field distributions in the magnetospheric-ionospheric auroral region, *J. Geophys. Res., 83*, A3, 629-642.

Comfort, R. H. (1988), The magnetic mirror force in plasma fluid models, in *Modeling Magnetospheric Plasma, Geophys. Monogr.*, vol. 44, edited by T. E. Moore and J. H. Waite Jr., pp 52-53, AGU, WAshington, D. C.

Ergun, R. E., C. W. Carlson, J. P. McFadden, F. S. Mozer and R. J. Strangeway (2000), Parallel electric fields in discrete arcs, *Geophys. Res. Lett., 27*, 24, 4053-4056.

457 Ergun, R. E., Y. J. Su, C. W. Carlson, J. P. McFadden, F. S. Mozer, D. L. Newman,
458 M. V. Goldman and R. J. Strangeway (2001), Direct observation of localized parallel
459 electric fields in a space plasma, *Phys. Rev. Lett., 87*, 4, 045003, doi: 10.1103/Phys-
460 RevLett87.045003.

461 Ergun, R. E., L. Andersson, D. S. Main, Y. J. Su, C. W. Carlson, J. P. McFadden and F. S.
462 Mozer (2002), Parallel electric fields in the upward current region of the aurora: Indirect
463 and direct observations, *Phys. Plasmas, 9*, 9, 3685-3694, doi: 10.1063/1.1499120.

464 Ergun, R. E., L. Andersson, D. Main, Y. J. Su, D. L. Newman, M. V. Goldman, C. W.
465 Carlson, J. P. McFadden and F. S. Mozer (2002), Parallel electric fields in the upward
466 current region of the aurora: Numerical solutions, *Phys. Plasmas, 9*, 9, 3695-3704, doi:
467 10.1063/1.1499121.

468 Ergun, R. E., L. Andersson, D. Main, Y. J. Su, D. L. Newman, M. V. Goldman, C.
469 W. Carlson, J. P. McFadden and F. S. Mozer (2004), Auroral particle acceleration by
470 strong double layers: The upward current region, *J. Geophys. Res., 109*, A12220, doi:
471 10.1029/2004JA010545.

472 Hull, A. J., J. W. Bonnell, F. S. Mozer and J. D. Scudder (2003), A statistical study
473 of large-amplitude parallel electric fields in the upward current region of the auroral
474 acceleration region, *J. Geophys. Res., 108*, A1, 1007, doi:10.1029/2001JA007540.

475 Hull, A. J., J. W. Bonnell, F. S. Mozer, J. D. Scudder and C. C. Chaston (2003), Large
476 parallel electric fields in the upward current region of the aurora: Evidence for ambipolar
477 effects, *J. Geophys. Res., 108*, A6, 1265, doi:10.1029/2002JA009682.

478 Knight, S. (1973), Parallel electric fields, *Planet. Space Sci., 21*, 741-750.

Langmuir, I. (1929), The interaction of electron and positive ion space charges in cathode sheaths, *Phys. Rev., 33*, 954-989.

Miller, R. H., and G. V. Khazanov (1993), Self-consistent electrostatic potential due to trapped plasma in the magnetosphere, *Geophys. Res. Lett., 20*, 1331-1334.

Mozer, F. S., A. J. Hull (2001), Origin and geometry of upward electric fields in the auroral acceleration region, *J. Geophys. Res., 106*, A4, 576, 5763-5778.

Persson, H. (1963), Electric field along a magnetic line of force in a low-density plasma, *Phys. Fluids, 6*, 12, 1756-1759.

Persson, H. (1963), Electric field parallel to the magnetic field in a low-density plasma, *Phys. Fluids, 9*, 6, 1090-1098.

Rönnmark, K. (1999), Electron acceleration in the auroral current circuit, *Geophys. Res. Lett., 26*, 7, 983-986.

Stern, D. P. (1981), One-dimensional models of quasi-neutral parallel electric fields, *J. Geophys. Res., 86*, A7, 5839-5860.

Vedin, J. and K. Rönnmark (2004), A linear auroral current-volatge relation in fluid theory, *Ann. Geophys., 22*, 1719-1728, doi:1432-0576/ag/2004-22-1719.

Vedin, J. and K. Rönnmark (2005), Electron pressure effects on driven auroral Alfvén waves, *J. Geophys. Res., 110*, A01214, doi:10.1029/2004JA010610.

Vedin, J. and K. Rönnmark (2006), Particle-fluid simulation of the auroral current circuit, *J. Geophys. Res., 111*, A12201, doi:10.1029/2006JA011826.

Vedin, J. and K. Rönnmark (2007), Parallel electric fields; variations in space and time on auroral field lines, *J. Plasma Physics, 74*, 53-64, doi:10.1017/S0022377807006538.

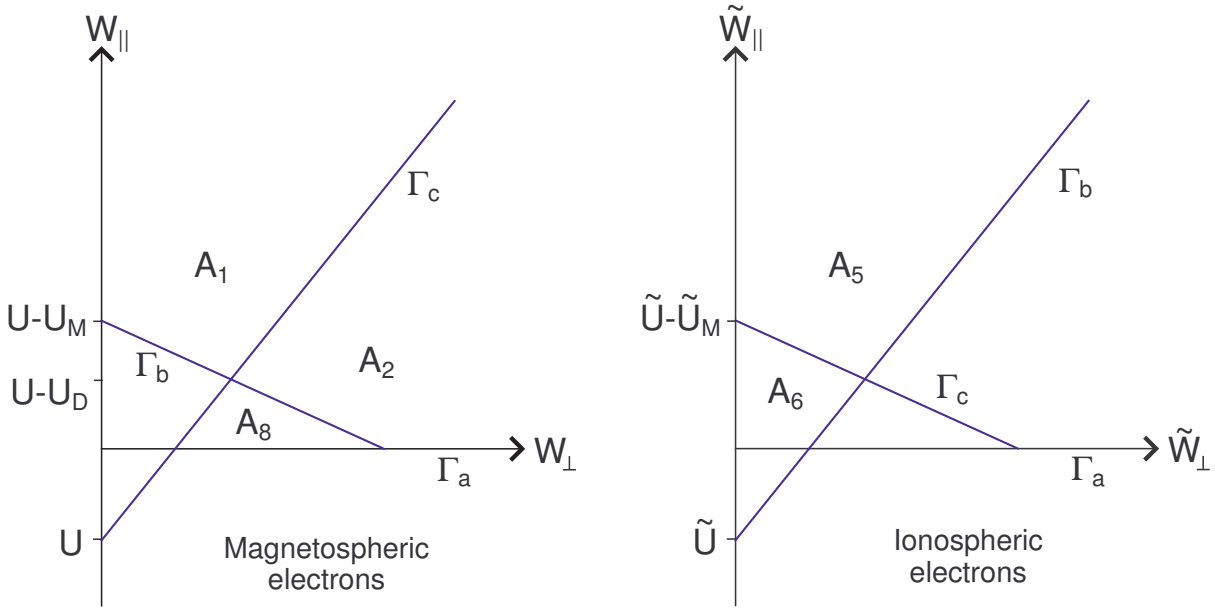

Figure 1. Regions of phase space populated by electrons, originating from the ionosphere (right panel) and magnetosphere (left panel), at an arbitrary point ζ where the electrostatic potential is $U(\zeta)$. Particles in regions A_1 and A_5 travel the length of the flux tube without mirroring, while those in regions A_2 and A_6 mirror. Particles in region A_8 are trapped between the magnetic mirror and electrostatic forces. Figure adapted from Figure 2 of *Boström* [2004].

501 Whipple, E. C., Jr. (1977), The signature of parallel electric fields in a collisionless plasma,
502 *J. Geophys. Res., 82*, 10, 1525-1531, doi:10.1029/JA082i010p01525.
503 Wright, A. N., W. Allan, M. S. Ruderman and R. C. Elphic (2002), The dynamics of cur-
504 rent carriers in standing Alfvén waves: Parallel electric fields in the auroral acceleration
505 region, *J. Geophys. Res., 107*, A7, doi:10.1029/2001JA900168.
506 Wright, A. N., and A. W. Hood (2003), Field-aligned electron acceleration in Alfvén
507 waves, *J. Geophys. Res., 108*, A3, 1135, doi:10.1029/2002JA009551.

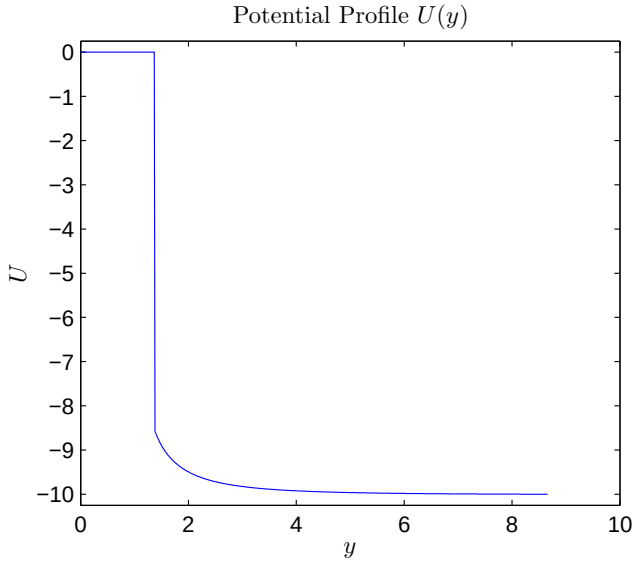

Figure 2. Plot of the electric potential variation U as a function of the field-aligned coordinate y, for the whole spatial length of the flux tube. The plot exhibits the three main regions of interest: earthward of the potential jump (pre-potential jump); within the present double layer (within the potential jump); and magnetospheric end of the jump (the post-potential jump). Note that the potential variation in the pre-jump region and within the potential jump varies on a scale that cannot be resolved by this plot (see figure 3 for further details).

Table 1. Key dimensionless parameters for numerical simulations. The bottom half of the table lists the potential jump conditions obtained as part of the quasi-neutral solution calculated from the parameters listed in the top half of the table.

Quantity	Value
ζ_M	1000
U_M	-10
τ	1×10^{-3}
ν	3×10^{3}
ζ_j	13.47
U_{j1}	-2.31×10^{-3}
U_{j2}	-8.53

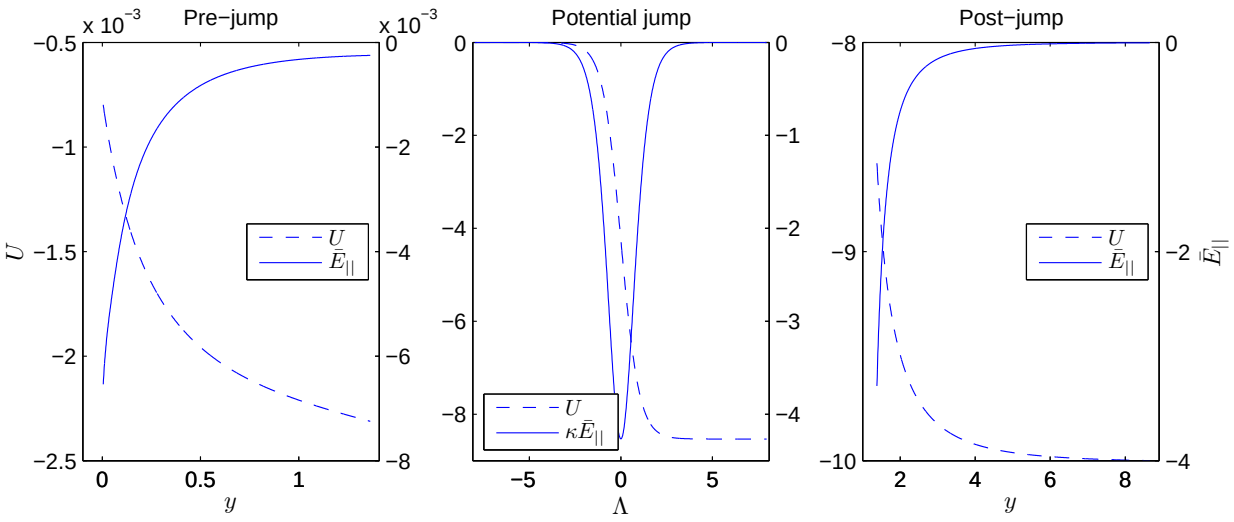

Figure 3. Plot of the electric potential variation U in the three regions of interest: earthward of the potential jump (pre-potential jump); within the present double layer (within the potential jump); and magnetospheric end of the jump (the post-potential jump). The dashed (solid) curve is the electric potential (parallel electric field), in all subplots the left-hand axis (right-hand axis) corresponds to the electric potential (parallel electric field). Pre- and post-potential jump the variation is a function of the field-aligned coordinate y; within the potential jump the variation is a function of a dimensionless spatial parameter Λ. Note that within the potential jump the plotted parallel electric field is $\kappa\bar{E}_{\|}$ where $\kappa = R_0/R_E$, R_0 being the typical width of the double layer.

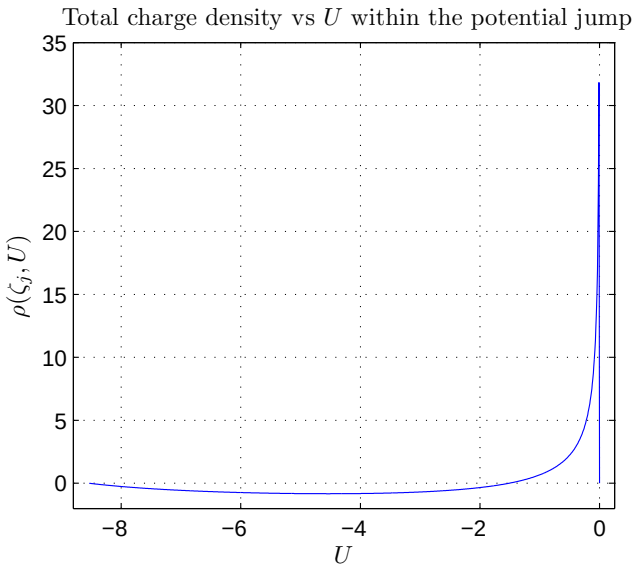

Figure 4. The total (dimensionless) charge density (all species α including ions) as a function of potential within the potential jump from U_{j1} to U_{j2}. The positive and negative charge distribution within the double layer balance and $\int_{U_{j1}}^{U_{j2}} \rho(\zeta_j, U)\mathrm{d}U = 0$

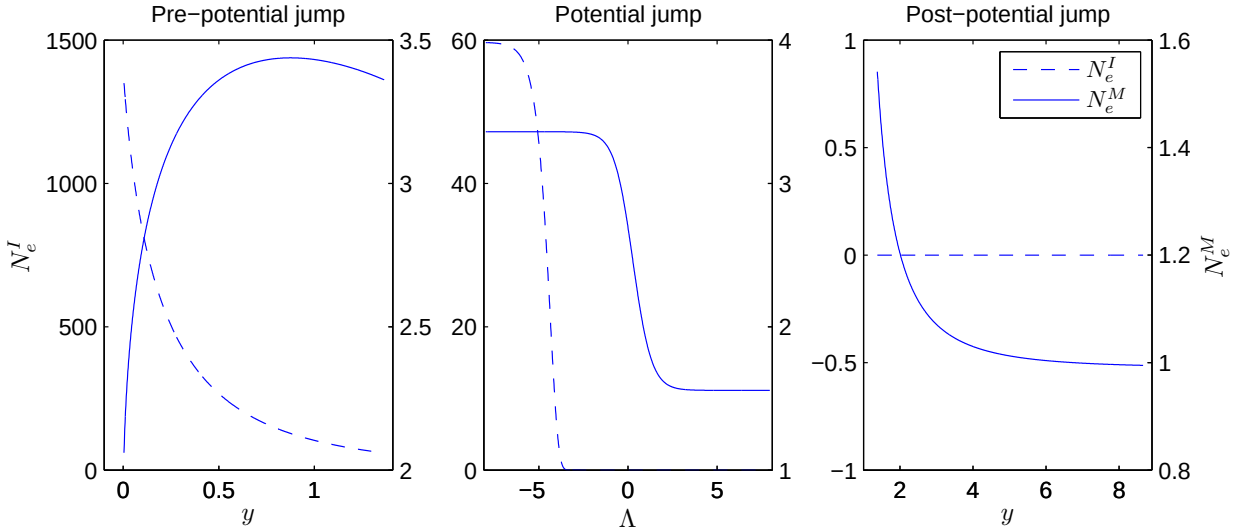

Figure 5. Variation of the magnetospheric (N_e^M - solid curve) and ionospheric electron number density (N_e^I - dashed curve) as a function of position y along the flux tube and position Λ within the potential jump. Note that in the three subplots the left-hand axis (right-hand axis) corresponds to N_e^I (N_e^M).

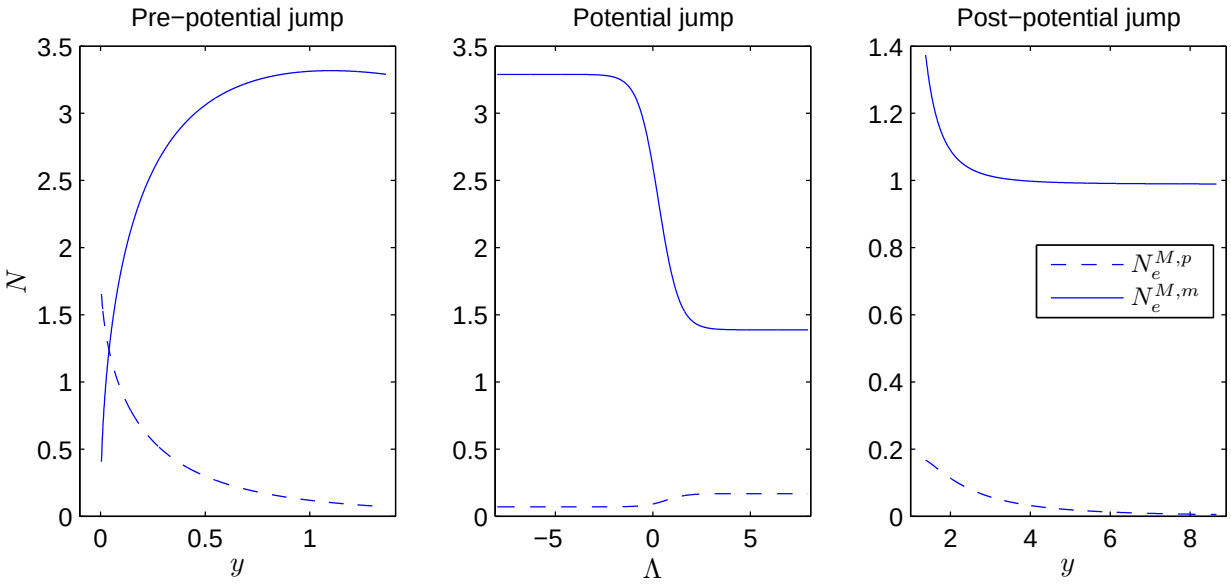

Figure 6. The magnetospheric electron number density (N_e^M) decomposed into its mirroring ($N_e^{M,m}$-solid curve) and precipitating populations ($N_e^{M,p}$-dashed curve). $N_e^{M,m}$ and $N_e^{M,p}$ are plotted as functions of y (and Λ within the potential jump). The plot clearly shows what populations that make up N_e^M dominate in what regions.

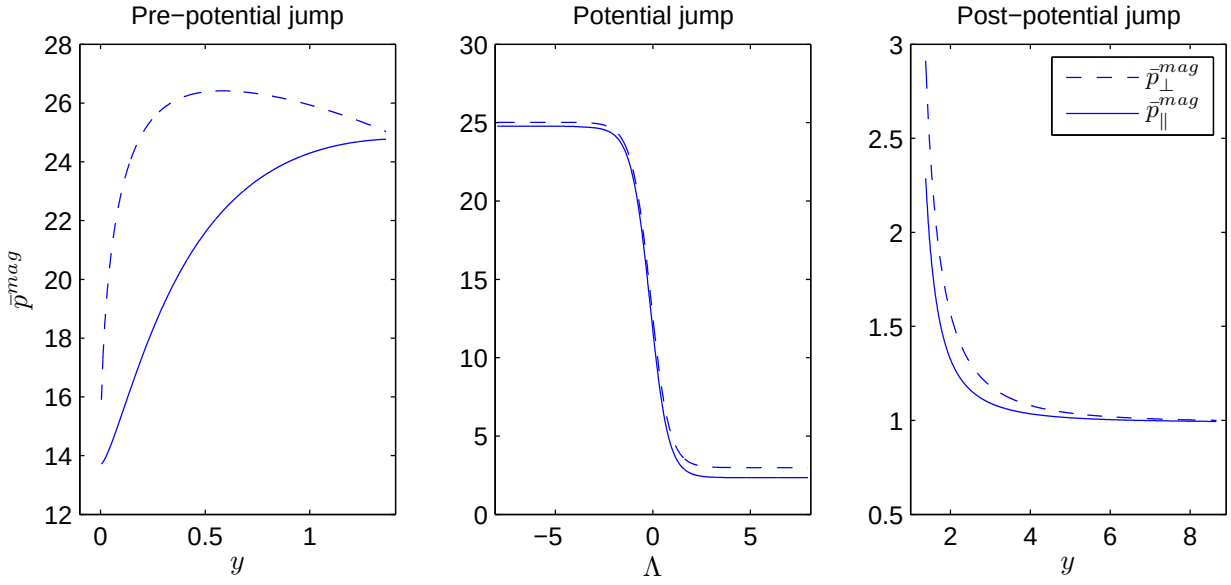

Figure 7. Magnetospheric parallel ($\bar{p}_\parallel^{\rm mag}$- solid curve) and perpendicular ($\bar{p}_\perp^{\rm mag}$- dashed curve) pressures plotted as a function of y pre- and post-potential jump and as function of Λ within the potential jump.

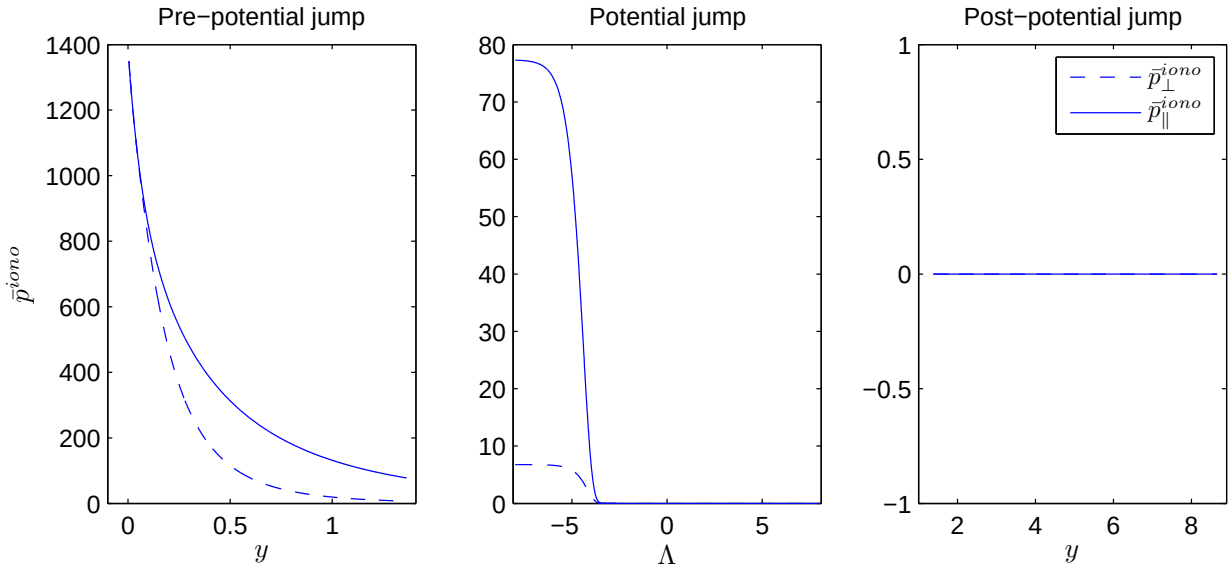

Figure 8. Ionospheric parallel ($\bar{p}_{\parallel}^{\text{iono}}$- solid curve) and perpendicular ($\bar{p}_{\perp}^{\text{iono}}$- dashed curve) pressures plotted earthward of the potential jump, within the jump and on the magnetospheric side of the jump.

Table 2. This table lists the important quantities used in the preceding work. It shows the dimensional quantity (x), its non-dimensional counterpart ($\hat{x}$) and its characteristic value (x_0) such that $\hat{x} = x/x_0$.The following symbols have the meaning: T_M is the magnetospheric plasma temperature; T_I is the ionospheric plasma temperature; R_E is the radius of the Earth; and k_B is the Boltzmann constant.

Quantity	Non-dimensional form	Characteristic value	Description
$v_{\parallel,\perp}$	$u_{\parallel,\perp}$	$\sqrt{k_B T_M/m}$	magnetospheric parallel (perpendicular) guiding
$v_{\parallel,\perp}$	$\tilde{u}_{\parallel,\perp}$	$\sqrt{k_B T_I/m}$	ionospheric parallel (perpendicular) guiding centr
$(mv_{\parallel,\perp}^2)/2$	$W_{\parallel,\perp}$	$k_B T_M$	magnetospheric parallel (perpendicular) kinetic e
$(mv_{\parallel,\perp}^2)/2$	$\tilde{W}_{\parallel,\perp}$	$k_B T_I$	ionospheric parallel (perpendicular) kinetic energ
ϕ	U	$k_B T_M/e$	electric potential normalised to magnetospheric p
ϕ	$\tilde{U}$	$k_B T_I/e$	electric potential normalised to ionospheric plasn
$E_{\parallel}$	$\bar{E}_{\parallel}$	$k_B T_M/(R_E e)$	parallel electric field
j	i	$n_0 e\sqrt{k_B T_M/m}$	current density
$p_{\parallel,\perp}^{\text{mag}}$	$\bar{p}_{\parallel,\perp}^{\text{mag}}$	$(k_B T_M n_0)^{-1}$	parallel (perpendicular) magnetospheric pressure
$p_{\parallel,\perp}^{\text{iono}}$	$\bar{p}_{\parallel,\perp}^{\text{iono}}$	$(k_B T_I n_0)^{-1}$	parallel (perpendicular) magnetospheric pressure
f_M	$\bar{f}_M$	$n_0(k_B T_M/m)^{-3/2}$	magnetospheric electron distribution function
f_I	$\bar{f}_I$	$n_0(k_B T_I/m)^{-3/2}$	ionospheric electron distribution function
n	N	n_0	number density, n_0 is the magnetospheric source

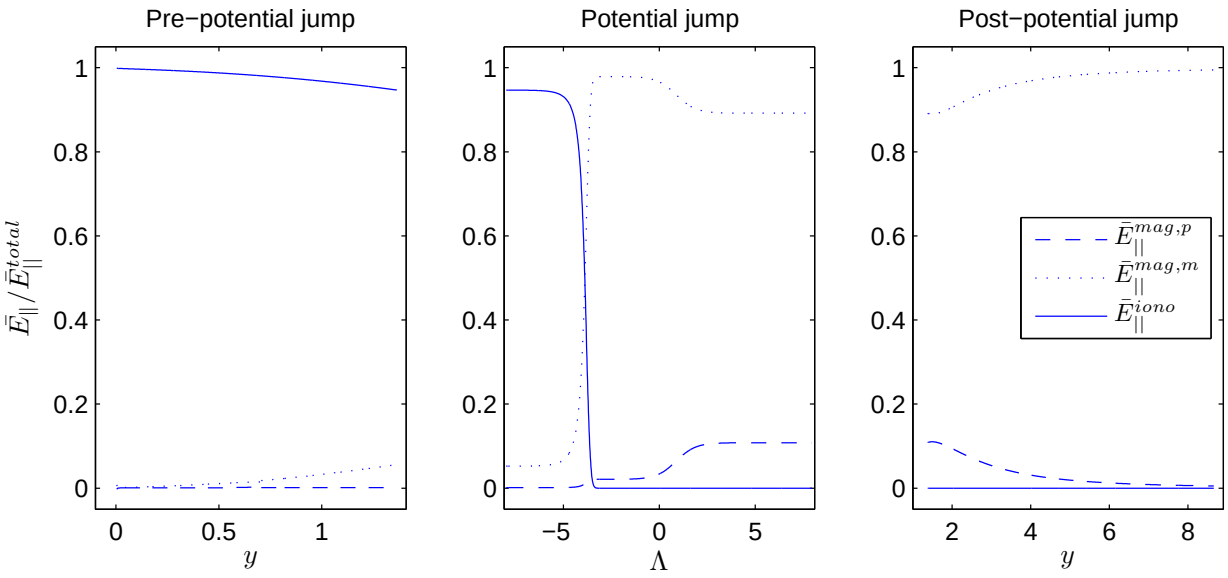

Figure 9. Contributions to the parallel electric field $\bar{E}_{\|}$ from the ionospheric ($\bar{E}_{\|}^{\mathrm{iono}}$ - solid), magnetospheric mirroring ($\bar{E}_{\|}^{\mathrm{mag,m}}$ - dot) and magnetospheric precipitating ($\bar{E}_{\|}^{\mathrm{mag,p}}$ - dash) populations. Note that these contributions are normalised to the total parallel electric field $\bar{E}_{\|}^{\mathrm{total}}$ at each y (or Λ) shown in Figure 3 (to aid in the visualisation of the data). In the pre-jump region the ionospheric population supports the parallel electric field. Within the potential jump when $N_e^I \approx N_e^M$ ($\Lambda \approx -4$) the magnetospheric mirroring population suddenly becomes the dominant contributor to $\bar{E}_{\|}$. In the post-jump region, the magnetospheric mirroring population remains the dominant species balancing $\bar{E}_{\|}$.

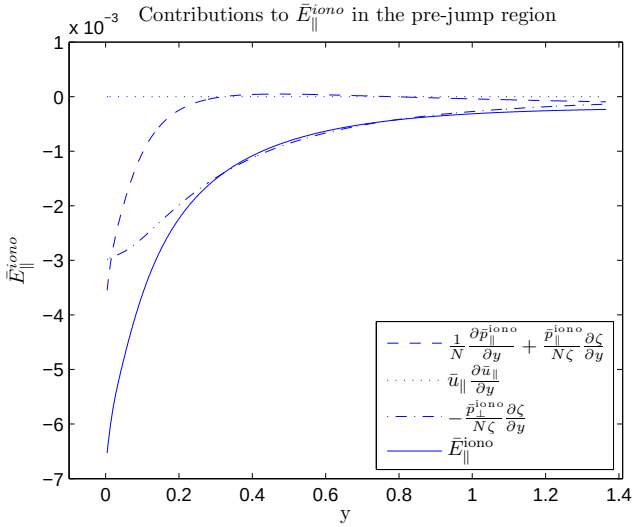

Figure 10. Contributions to $\bar{E}_\parallel^{\rm iono}$ from the moments of the the ionospheric electron distribution. These correspond to: the parallel pressure gradient plus the pressure force associated with the magnetic inhomogeneity (dash); the electron fluid acceleration (dot); the magnetic mirror force (dot-dash); and $\bar{E}_\parallel^{\rm iono}$ (solid). Contributions are plotted as a function of y in the pre-potential jump region. In most of this region the magnetic mirror force is the main effect balancing the parallel electric field.

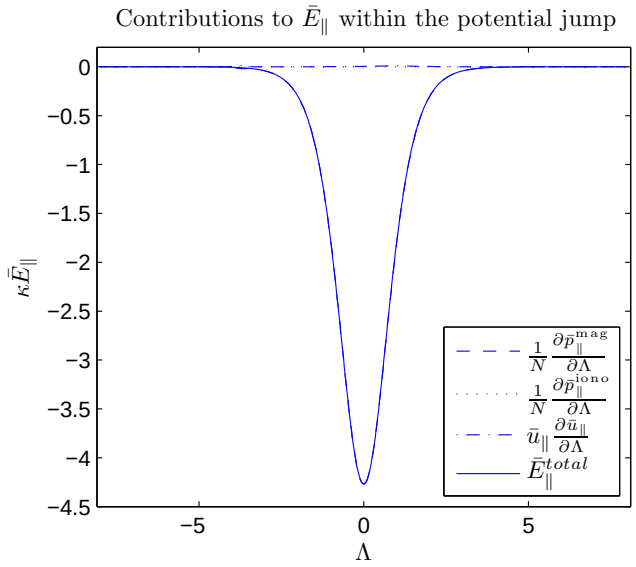

Figure 11. Contributions to $\bar{E}_\parallel$ from the moments of the moments of the electron distribution. These correspond to: the magnetospheric parallel pressure gradient (dash); the ionospheric parallel pressure gradient (dot); the electron fluid acceleration (dot-dash); and $\bar{E}_\parallel$ (solid). Contributions are plotted as a function Λ within the potential jump. The contributions from the electron fluid acceleration and the ionospheric parallel pressure gradient are negligibly small, leaving the magnetospheric parallel pressure gradient to balance the parallel electric field. As a result the plot of $\bar{E}_\parallel$ (solid) is indistinguishable from that of the magnetospheric parallel pressure gradient (dash).

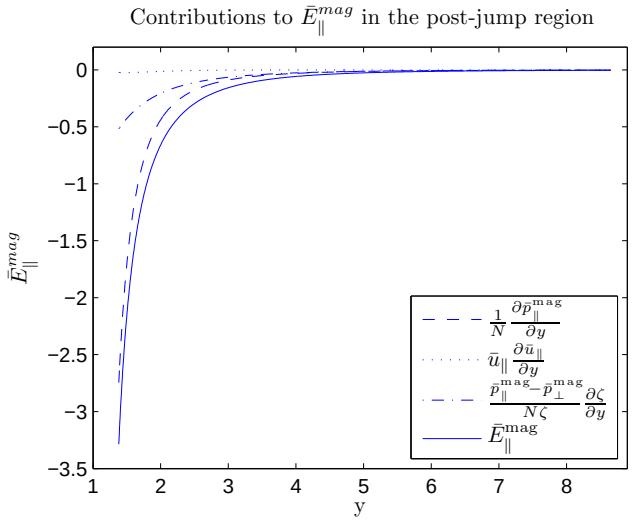

Figure 12. Contributions to $\bar{E}_{\parallel}^{\mathrm{mag}}$ from the moments of the the magnetospheric electron distribution. These correspond to: the parallel pressure gradient (dash); the electron fluid acceleration (dot); the magnetic inhomogeneity (dot-dash); and $\bar{E}_{\parallel}^{\mathrm{mag}}$ (solid). Contributions are plotted as a function of y in the post-potential jump region, where the magnetospheric parallel pressure gradient is the primary contributor to $\bar{E}_{\parallel}$.